

See discussions, stats, and author profiles for this publication at: <https://www.researchgate.net/publication/255787961>

Fibrinogen Mono layer Characterization by Colloid Deposition

ARTICLE *in* LANGMUIR · AUGUST 2013

Impact Factor: 4.46 · DOI: 10.1021/la402628x · Source: PubMed

CITATIONS

4

READS

40

4 AUTHORS, INCLUDING:



[Zbigniew Adamczyk](#)

Akademickie Centrum Komputerowe CYFRON...

177 PUBLICATIONS 3,724 CITATIONS

SEE PROFILE



[Monika Wasilewska](#)

Instytut Katalizy i Fizykochemii Powierzchni i...

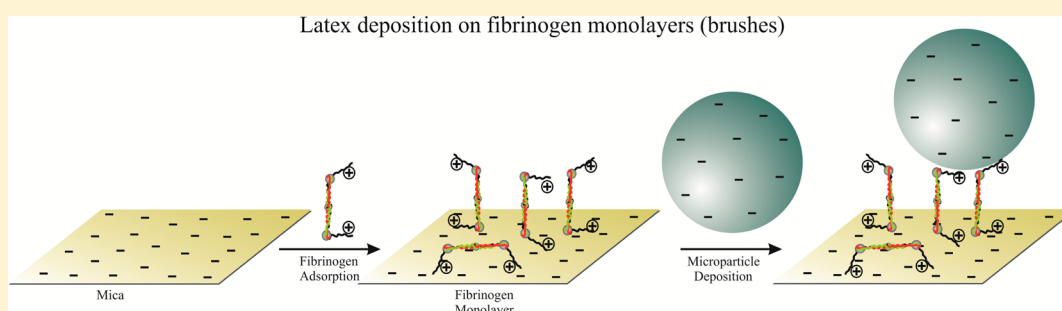
17 PUBLICATIONS 348 CITATIONS

SEE PROFILE

Fibrinogen Monolayer Characterization by Colloid Deposition

Małgorzata Nattich-Rak, Zbigniew Adamczyk,* Monika Wasilewska, and Marta Sadowska

Institute of Catalysis and Surface Chemistry, Polish Academy of Science, Niezapominajek 8, 30-239 Cracow, Poland



ABSTRACT: Colloid particle deposition was applied to characterize bovine and human fibrinogen (Fb) monolayers on mica produced by controlled adsorption under diffusion transport at pH 3.5. The surface concentration of Fb was determined by AFM enumeration of single molecules adsorbed over the substrate surface. The electrokinetic properties of Fb monolayers for various ionic strength were studied using the in situ streaming potential measurements. It was shown that Fb adsorbs irreversibly on mica for a broad range of ionic strength of 4×10^{-4} to 0.15 M, NaCl. The overcharging of initially negative mica surface occurred for fibrinogen surface concentrations higher than $1400 \mu\text{m}^{-2}$. The orientation of fibrinogen molecules in the monolayers was evaluated by the colloid deposition method involving negatively charged polystyrene latex microspheres, 820 nm in diameter. An anomalous deposition of negative latex particles on substrates exhibiting a negative zeta potential was observed, which contradicts the mean-field DLVO predictions. Measurable deposition was observed even at low ionic strength where the minimum approach distance of latex particles to the interface exceeds 70 nm (for 6×10^{-4} M NaCl). This confirms that, at this pH, fibrinogen molecules adsorb end-on on mica assuming extended conformations with the positive charge located mostly in the end part of the αA chains. This agrees with previous experimental and theoretical results discussed in the literature (Santore, M. M.; Wertz Ch. F. Protein spreading kinetics at liquid-solid interfaces via an adsorption probe method. *Langmuir* **2005**, *21*, 10172–10178 (experimental); Adamczyk, Z.; Barbasz, J.; Cieřla, M.; Mechanisms of fibrinogen adsorption at solid substrates. *Langmuir*, **2011**, *25*, 6868–6878 (theoretical)). This unusual latex deposition on Fb monolayers was quantitatively interpreted in terms of the model developed in ref 55 (Jin, X.; Wang, N. H. L.; Tarjus, G.; Talbot, J. Irreversible adsorption on nonuniform surfaces: the random site model. *J. Phys. Chem.* **1993**, *97*, 4256–4258). It was concluded that the colloid deposition method is an efficient tool for revealing protein adsorption mechanisms at solid/electrolyte interfaces.

1. INTRODUCTION

Adsorption of fibrinogen on various substrates is one of the most extensively studied topic because of the fundamental role of its monolayers in platelet and red blood cell adhesion, leucocyte binding, thrombosis, angiogenesis, inflammatory response, tumor growth, fouling of artificial organs, and so forth.^{1–5}

From a chemical point of view, the fibrinogen molecule is a symmetric dimer composed of three identical pairs of polypeptide chains, refereed to traditionally as $\text{A}\alpha$, $\text{B}\beta$, and γ chains.^{6,7} They are coupled in the middle of the molecule through a few disulfide bridges forming a central nodule (see Table 1). The longest $\text{A}\alpha$ chain is composed of 610 amino acids, the $\text{B}\beta$ chain comprises 460 amino acids, and the γ chain 411 amino acids. Accordingly, the molecular mass of the fibrinogen molecule equals to 337 897 Da.⁸ Moreover, from the chemical structure, it can be deduced that a considerable part of the $\text{A}\alpha$ chains extends from the core of the molecule forming two polar appendages (arms), each having molecular mass

equal to 42 300 Da.⁷ These end parts of these the $\text{A}\alpha$ chains are called the αC domains.⁹ However, these chains are collapsed under vacuum conditions and are not clearly visible in the crystallographic structure of fibrinogen (see Table 1).

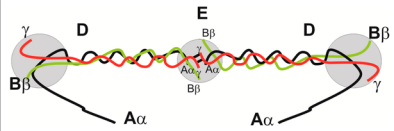
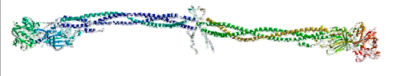
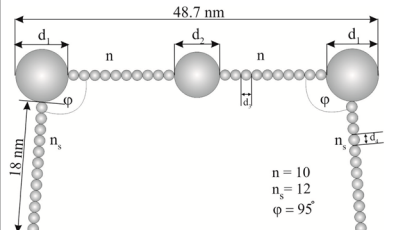
Reliable information about fibrinogen's geometrical dimensions and conformations stem from electron microscopy^{10–13} and atomic force microscopy (AFM)^{9,14–20} imaging of single molecules deposited on various substrates. It was established that the molecule has a colinear, trinodular shape with a total length of 47.5 nm. The two equal end domains of rather irregular shape are approximated by spheres having the diameter of 6.5 nm; and the middle domain has a diameter of 5 nm. This indicates that the fibrinogen molecule is highly anisotropic and elongated, characterized by the length to width ratio above 10. It should be mentioned that these dimensions

Received: July 11, 2013

Revised: August 11, 2013

Published: August 12, 2013

Table 1. Model Shapes of the Fibrinogen Molecule

Model	Shape of Molecule	Refs.
Chemical		$M_w = 337,897 (8)$
Crystallographic		(59)
Bead Model B		(58)

were determined under dry or vacuum conditions, where the molecule is likely to change its native conformation occurring in the electrolyte solutions, because of considerable dehydration.

Numerous experimental studies were also devoted to fibrinogen adsorption on various substrates. They were mainly focused on determining adsorption isotherms for various conditions by measuring the maximum coverage as a function of the bulk concentration of the protein.^{20–26} Most of the works were performed at pH 7.4 and ionic strength of 0.15 M, NaCl, pertinent to physiological conditions.^{19–26} For example, precise kinetic measurements of fibrinogen adsorption on silicon and modified glass surfaces forming parallel-plate channels were performed by Santore and Wertz^{25,26} using in situ TIRF and AFM techniques. On the other hand, the influence of pH and ionic strength on fibrinogen adsorption was systematically studied by Ortega-Vinuesa et al.^{14,15} by ellipsometry. However, using these experimental techniques, one cannot derive relevant information about orientation of fibrinogen molecules in monolayers in the normal direction to the interface, which is of vital practical significance.

Some hints concerning fibrinogen orientation in monolayers on solid substrates were gained from the ingenious experiments performed by Santore and Wertz.²⁶ They measured spreading kinetics of fibrinogen molecules adsorbed on hydrophobic and hydrophilic surfaces using the adsorption probe technique. A significant increase in the footprint area of molecules adsorbed on hydrophobized surfaces was observed. This was interpreted in terms of the transition from end-on to side-on orientation of adsorbed fibrinogen molecules.

Analogously, in the work of Dyr and Suttner,²⁷ it was shown via SPR measurements (surface plasmon resonance) that the results of antibody binding to fibrinogen monolayers on gold can only be explained assuming the end-on orientation of molecules. However, quantitative evidence of this effect was not provided.

The prevailing end-on conformations of fibrinogen molecules adsorbed on negatively charged latex particles (820 nm in diameter) at pH 3.5 was confirmed in ref 28. This was deduced by comparing the maximum coverage of fibrinogen determined

by microelectrophoretic and concentration depletion methods with the theoretical predictions derived in ref 29 for various molecule orientations in monolayers. The formation of dense, brushlike fibrinogen monolayers on latex particles was also confirmed by DLS measurements of the hydrodynamic diameter of particles.²⁸

However, from the above cited works, one cannot extract any quantitative information about fibrinogen molecule orientations under transient states where incomplete monolayers on solid substrates are formed. Therefore, in this work, an efficient method of analyzing fibrinogen monolayers on solid substrates under the wet, in situ conditions is used. The technique, referred to as the colloid deposition, consists of unspecific, electrostatically driven deposition of colloid particles onto polyelectrolyte or protein monolayers.^{30–34} A major advantage of this method is that the coverage of colloid can be directly determined via optical microscope or AFM imaging. In this way, a unique functional dependence between the protein and the colloid particle coverages can be experimentally derived. By exploiting these data and deriving thorough electrokinetic characteristics of protein covered substrates, one can gain reliable clues about the validity of the classical DLVO theory, which is based on the mean field concept.

Another advantage of the colloid deposition method is that the minimum approach distance between the particles and interfaces (bearing the same sign of surface charge) can be adjusted continuously within broad limits by ionic strength variations. By comparing results of these experiments with the recent theoretical predictions,²⁹ one can quantitatively determine the number of fibrinogen molecules adsorbed in the end-on orientation for broad coverage range. This allows one to reveal the fibrinogen adsorption mechanism at solid substrates that is the main goal of this work. In contrast to previous works, we will study and compare human and bovine fibrinogens, that broadens the range of applicability of the result obtained.

It should also be mentioned that the colloid particle deposition processes on fibrinogen monolayers can mimic biofilm formation, a critical phenomenon inducing thrombosis, angiogenesis, inflammatory response, fouling of artificial organs,

Table 2. Physicochemical Parameters Determined for Mica, Fibrinogens (Bovine and Human) and Latex at pH 3.5^a

NaCl concentration [M]	mica		fibrinogen (bovine, human)			latex (L800)		
	ζ [mV]	σ_0 [e nm ⁻²]	μ_e [$\mu\text{m cm (Vs)}^{-1}$]	ζ [mV]	N_c	μ_e [$\mu\text{m cm (Vs)}^{-1}$]	ζ_1 [mV]	σ_0 [e nm ⁻²]
3×10^{-4}	-66	-0.020	$2.1 \pm 0.1, 2.0 \pm 0.1$	40, 38	24, 22	-5.7 ± 0.2	-80	-0.029
6×10^{-4}	-63	-0.028	$1.9 \pm 0.1, 1.8 \pm 0.1$	35, 33	21, 20	-6.0 ± 0.2	-82	-0.043
10^{-3}	-63	-0.036	$1.8 \pm 0.1, 1.7 \pm 0.1$	33, 31	20, 19	-6.6 ± 0.2	-89	-0.064
10^{-2}	-52	-0.088	$1.7 \pm 0.1, 1.5 \pm 0.1$	29, 26	19, 17	-7.7 ± 0.2	-100	-0.25

^a

$$\sigma_0 = \frac{(8ekTn_b)^{1/2}}{0.16} \sinh\left(\frac{e\zeta}{2kT}\right), \quad N_c = \frac{30\pi\eta}{1.6} d_t \mu_e$$

where d_t is expressed in nm and μ_e in [$\mu\text{m cm (V s)}^{-1}$].

and so forth. Besides the significance for basic science, the obtained results allow one to specify conditions for preparing fibrinogen monolayers of precisely known coverage and orientations of molecules having potential applications for biosensing and immunological assays.

2. MATERIALS AND METHODS

Fibrinogens from bovine and human blood plasmas, fractions I, type IV in the form of crystalline powders containing 65% protein, 25% sodium chloride, and 15% sodium citrate (Sigma F4753) were used in this work. The purity of fibrinogen solutions was checked by dynamic surface tension measurements after acquiring supernatant solution by membrane filtration.

Fibrinogen solutions were prepared by dissolving appropriate amounts of crystalline powders under gentle stirring at pH 3.5 and 310 K in a high purity distilled water. Afterward, the suspension was filtered through the Millex-GS 0.45 μm filter to eliminate aggregates and impurities and the bulk concentration of fibrinogen was spectrophotometrically determined using BCA (bicinchoninic acid) protein assays.³⁵ The stock solutions obtained in this way (having a concentration of 600–800 mg L⁻¹) were diluted to a desired bulk concentration, usually 0.1–10 mg L⁻¹, prior to each experiment. The pH of the solution was adjusted by the addition of HCl (the use of buffers was avoided to eliminate the possibility of a specific adsorption of ions), and the ionic strength was adjusted by the addition of NaCl.

Water was purified by using a Milipore Elix 5 apparatus. Chemical reagents (sodium chloride, hydrochloric acid) were commercial products of Sigma-Aldrich and used without further purification. The temperature of experiments was kept at a constant value equal to 298 ± 0.1 K.

Negatively charged sulfonate polystyrene latex synthesized in our laboratory according to the Goodwin procedure³⁶ were used in colloid deposition experiments. The stock suspension of latex of a well-defined concentration, determined by densitometry and the dry weight method, was diluted prior to deposition experiments to a desired weight concentration of 10–20 g L⁻¹.

Ruby muscovite mica obtained from Continental Trade was used as a substrate. The solid pieces of mica were freshly cleaved into thin sheets prior to each experiment.

The diffusion coefficients of fibrinogens were determined by dynamic light scattering (DLS) using the Zetasizer Nano ZS instrument from Malvern.

The electrophoretic mobilities of fibrinogen and latex particles were measured using the laser doppler velocimetry (LDV) technique. The margin of error of the electrophoretic mobility measurements was $\pm 2\%$.

AFM measurements of fibrinogen monolayers on mica were carried out using the NT-MDT Solver PRO device with the SMENA SFC050L scanning head. The measurements were performed in semicontact mode using a silicon probe (polysilicon cantilevers with resonance frequencies of 240 kHz $\pm 10\%$ or 140 kHz $\pm 10\%$, a typical tip curvature of 10 nm, and a cone angle less than 20°).

The latex particle size, as a function of ionic strength and pH, was determined using a laser diffractometer (Particle Size Analyzer LS 13 320 Beckman Coulter) with an accuracy of few percent and independently by the DLS method using the Malvern Zetasizer Nano ZS instrument.

Streaming potential measurements were carried out using a homemade apparatus, exploiting the parallel-plate channel flow, according to the procedure previously described.^{37–39}

Fibrinogen adsorption runs were performed in a diffusion cell having a volume of 40 mL, filled with the protein suspension of a desired concentration and ionic strength. Freshly cleaved mica sheets (usually 4–8) were vertically placed in the cell for a desired time. Afterward, some of the mica sheets (2–4) were rinsed with a stream of pure buffer solution for 30 s and dried under a gentle stream of nitrogen. Afterward, the number concentration of fibrinogen was directly determined by AFM examination.

The remaining mica sheets were used in latex deposition experiments performed in another diffusion cell, having the dimensions of $2 \times 2 \times 5$ cm³. It was filled with the latex suspension. Wet mica sheets, precovered by fibrinogen monolayers as described above, were vertically immersed into the latex suspension. Particle deposition proceeded over a desired time (24 h). The true coverage of particles was determined by a direct optical microscope counting under wet conditions, as described in our previous works.^{37,38,40,41} Particles were counted over 10–20 equal sized areas chosen at random over mica sheets. The net number of considered particles was ca. 2000, which ensured these measurements a relative precision below 2%, as determined by variance analysis. It is worthwhile mentioning that the coverage was determined in absolute terms, that is, $\Theta_1 = S_1 N_1$, where N_1 is the average surface concentration of particles (number of particles per unit area) and $S_1 = \pi d_1^2/4$ is the cross section of the particle (d_1 is the particle radius).

However, because of multiple scattering, the optical microscope method became less accurate for coverage exceeding 0.3. In this case, the AFM method (NT MDT Integra system) working in the semicontact mode under dry conditions was used to determine the surface concentration of particles and their coverage.

3. RESULTS AND DISCUSSION

3.1. Bulk Characteristics of Fibrinogens and the Substrate Surface. Physicochemical characteristics of fibrinogens and latex particles were initially determined. These comprised the diffusion coefficients, electrophoretic mobilities, and electrokinetic (zeta) potentials.

The average value of the diffusion coefficient D for the bovine fibrinogen was 2.1×10^{-7} cm² s⁻¹ for the ionic strength range of 10^{-3} – 10^{-2} M and for pH 3.5. For the ionic strength range of 10^{-3} – 3×10^{-4} M, the average value of D was 2.0×10^{-7} cm² s⁻¹ (pH 3.5). Similar diffusion coefficients (within error bounds of 5%) were also obtained for human fibrinogen. Knowing diffusion coefficients, the Stokes hydrodynamic

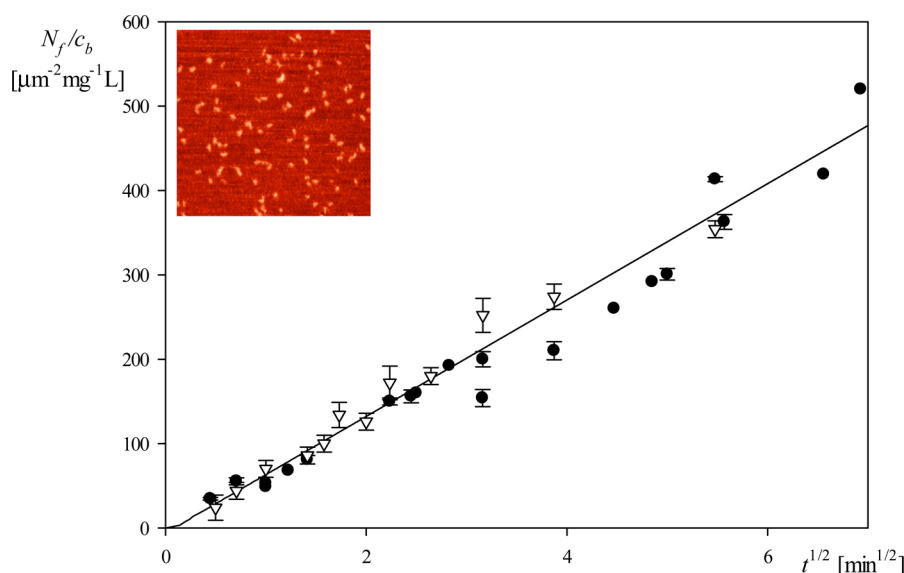


Figure 1. Dependence of the reduced surface concentration of fibrinogen N_f/c_b [$\mu\text{m}^{-2} \text{mg}^{-1} \text{L}$] on the square of the adsorption time $t^{1/2}$ [$\text{min}^{1/2}$], $I = 10^{-2} \text{ M}$, pH 3.5. The solid points denote experimental results obtained by a direct AFM enumeration for bovine fibrinogen, and the hollow points denote results obtained for human fibrinogen. The solid line shows exact theoretical results obtained using the RSA model. The inset shows the AFM image of a fibrinogen monolayer at surface concentration $N_f = 60 \mu\text{m}^{-2}$.

diameter d_f of fibrinogens was calculated using the dependence:⁴²

$$d_f = \frac{kT}{3\pi\eta D} \quad (1)$$

It was calculated from eq 1 that $d_f = 21.4 \text{ nm}$ for the ionic strength range of 3×10^{-4} to 10^{-3} M and 22.4 nm for the ionic strength range of 10^{-3} – 10^{-2} M .

Another parameter characterizing the electrokinetic charge of the protein is electrophoretic mobility μ_e , defined as the translation velocity of the molecule U over the electric field E , that is, $\mu_e = U/E$. This quantity was directly measured using the microelectrophoretic method. It was determined that for both fibrinogens μ_e was positive at pH 3.5, monotonically decreasing with ionic strength (see Table 2). Hence, for bovine fibrinogen and NaCl concentration of $3 \times 10^{-4} \text{ M}$, $\mu_e = 2.1 \times 10^{-8} \text{ m}^2 (\text{Vs})^{-1} = 2.1 \mu\text{m cm} (\text{Vs})^{-1}$ (the latter unit is commonly used in the literature). For the NaCl concentration of 10^{-2} M , $\mu_e = 1.7 \mu\text{m cm} (\text{Vs})^{-1}$. These values correspond to the zeta potential of fibrinogen molecules equal to 40 and 29 mV, respectively (calculated using the Henry model; see Table 2). Slightly smaller values of electrophoretic mobilities were measured under analogous ionic strength for the human fibrinogen.

As previously discussed,^{39,42} knowing μ_e , one can calculate the electrokinetic charge per molecule Q_c (expressed in Coulombs) from the Lorenz–Stokes relationship:

$$Q_c = 3\pi\eta d_f \mu_e \quad (2)$$

where η is the dynamic viscosity of the solvent (water). Knowing Q_c , the number of electrokinetic (uncompensated) charges per molecule N_c can be calculated from eq 2 considering that one elementary charge $e = 1.602 \times 10^{-19} \text{ C}$.

For NaCl concentrations of 3×10^{-4} and 10^{-2} , the average number of electrokinetic charges on the bovine fibrinogen molecule N_c was 24 and 19, respectively. For other ionic strengths, the calculated charges N_c are listed in Table 2.

Analogously, the bulk characteristics of the latex particles were carried out. The diffusion coefficient of particles was determined using the DLS method as a function of the ionic strength. From these data, the hydrodynamic diameter of latex d_l was calculated. For the NaCl concentration of $3 \times 10^{-4} \text{ M}$, the hydrodynamic diameter of latex particles was $820 \pm 15 \text{ nm}$, and for 10^{-2} M $d_l = 810 \pm 14 \text{ nm}$.

The zeta potentials of latex were -80 and -100 mV for the NaCl concentration of 3×10^{-4} and 10^{-2} M , respectively (pH 3.5). Knowing the zeta potential of latex particles, one can calculate the electrokinetic (uncompensated) charge using the Gouy–Chapman relationship for a symmetric 1:1 electrolyte.⁴²

$$\sigma_0 = \frac{(8\epsilon k T n_b)^{1/2}}{0.16} \sinh\left(\frac{e\zeta_l}{2kT}\right) \quad (3)$$

where σ_0 is the electrokinetic charge density of latex particles expressed in $e \text{ nm}^{-2}$, k is the Boltzmann constant, ϵ is the dielectric permittivity of water, n_b is the number concentration of the salt (NaCl) expressed in m^{-3} , and ζ_l is the zeta potential of latex.

Using the above zeta potential values, one obtains from eq 3 the following charge densities of latex particles: $\sigma_0 = -0.029$, -0.064 , and $-0.25 e \text{ nm}^{-2}$ for the NaCl concentration of 3×10^{-4} , 10^{-3} , and 10^{-2} M , respectively (see Table 2). On the other hand, the zeta potential of the mica substrate was determined via the streaming potential measurements performed in the parallel-plate channel cell according to the procedure described in refs 37–39. Knowing streaming potential, one can calculate the zeta potential of the interface using the Smoluchowski's equation and the electrokinetic charge density using eq 3. For and the ionic strength of $3 \times 10^{-4} \text{ M}$, the zeta potential of mica was -66 mV , for 10^{-3} M it was -63 mV , and for 10^{-2} M it was -52 mV (at pH 3.5).

These data indicate that fibrinogen Fb should adsorb on mica for pH = 3.5, due to favorable electrostatic interactions, because its zeta potential is positive and the zeta potential of mica is strongly negative.

3.2. Measurements of Fibrinogen Adsorption on Mica. Fibrinogen adsorption kinetics on mica was quantitatively evaluated by AFM imaging for lower coverage range and by streaming potential measurements for higher coverage range. In the former case, fibrinogen molecules were adsorbed under diffusion transport conditions on mica plates for a controlled period of time as described above. Afterward, the average number of adsorbed molecules per unit area of the interface (surface concentration) was determined by a direct AFM imaging.

It is interesting to mention that a similar AFM counting procedure of isolated fibrinogen molecules was applied by Tsapikouni and Missirilis⁴³ and in refs 20 and 25 in order to determine its coverage on mica for pH 7.4 and various ionic strength. The topology of fibrinogen monolayers on mica imaged by AFM for pH 3.5 and ionic strength of 10^{-2} M is shown in the inset of Figure 1. As can be observed, fibrinogen molecules appear as isolated entities, which facilitates their enumeration by a special image analyzing software.

For the sake of convenience, the surface concentration of fibrinogen is expressed as the number of molecules per one square micrometer and denoted hereafter denoted by N_f . Hence, by determining N_f as a function of adsorption time, kinetic runs can be obtained for various bulk fibrinogen concentration c_b and ionic strength. In Figure 1, such runs are presented for both fibrinogens (bovine and human) in the normalized form, that is, as the dependence of N_f/c_b on the square root of the adsorption time $t^{1/2}$ ($I = 10^{-2}$ M, pH 3.5). As can be seen, the experimental results obtain for bovine and human fibrinogens are identical within error bounds. Moreover, they can be well approximated by theoretical results (depicted by the solid line) stemming from the formula, pertinent to an irreversible, diffusion-controlled adsorption mechanism^{44,45}

$$\frac{N_f}{c_b} = 2 \left(\frac{D}{\pi} \right)^{1/2} t^{1/2} \quad (4)$$

where t is the adsorption time.

The validity of this formula proves that fibrinogen adsorption on mica at this pH is irreversible and bulk transport controlled with negligible surface transport resistance, this seems quite natural considering the strong electrostatic attraction between molecules and the oppositely charged mica substrate.

The results shown in Figure 1 also indicate that fibrinogen monolayers of well-controlled surface concentration can be produced via the diffusion adsorption procedure. This allows one to unequivocally interpret latex deposition experiments discussed later on aimed at determination of fibrinogen molecule orientation in the monolayers. It should be mentioned, however, that because of the AFM imaging limitations, one can derive reliable kinetic results for N_f smaller than $1000 \mu\text{m}^{-2}$. Therefore, the fibrinogen adsorption kinetics for higher coverages was studied by the streaming potential measurements, carried out under the wet, in situ, conditions. This excludes any conformation changes within fibrinogen monolayers induced by drying.

A primary kinetic run derived for ionic strength of 10^{-2} M is presented in Figure 2 as the dependence of the zeta potential of protein covered surface ζ on the square root of the adsorption time $t^{1/2}$. As can be seen, a steep, quasi-linear increase in the negative zeta potential of mica is observed and afterward, for $t^{1/2} > 3 \text{ min}^{1/2}$, the inversion of the zeta potential occurs. Consequently, the zeta potential becomes positive and for

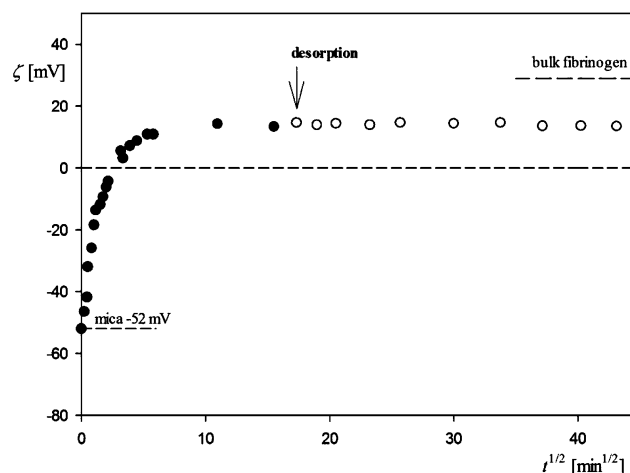


Figure 2. Bovine fibrinogen adsorption/desorption run expressed as the dependence of the zeta potential of fibrinogen covered mica ζ on the square root of the adsorption time $t^{1/2}$. The solid points denote experimental results obtained from the streaming potential measurements for pH 3.5, 10^{-2} M, NaCl, $c_b = 10 \text{ mg L}^{-1}$. The arrow and the hollow points show the desorption run where the cell was flushed with a pure electrolyte of the same pH and ionic strength.

higher coverage it approaches a saturation value, which is markedly lower than the bulk zeta potential equal to 29 mV for this ionic strength.

In order to prove irreversibility of fibrinogen adsorption, additional desorption experiments were performed under the in situ conditions. Accordingly, after forming the fibrinogen monolayer, at the time of 300 min ($t^{1/2} = 18 \text{ min}^{1/2}$), the cell was flushed with pure electrolyte solution of the same ionic strength and pH at the flow rate of 0.037 mL s^{-1} . As can be observed in Figure 2, the consecutive zeta potential changes were negligible suggesting minimum desorption of fibrinogen. Analogous runs were also performed for the human fibrinogen whose desorption was also negligible under these conditions.

Using the theoretical approach discussed in ref 46, one can convert the kinetic run shown in Figure 2 to the fibrinogen surface concentration vs the zeta potential relationship using the following transformation:

$$N_f = -\frac{N_{ch}}{C_i} \ln X(\zeta) \quad (5)$$

where N_{ch} is the scaling surface concentration, C_i is the dimensionless constant approaching for thin double-layers the limiting values of $C_i^0 = 10.2$, and $X_1(\zeta)$ is the normalized zeta potential given by

$$X(\zeta) = \frac{\zeta(t) - \zeta_p/\sqrt{2}}{\zeta_i - \zeta_p/\sqrt{2}} = \frac{\zeta(t) - \zeta_\infty}{\zeta_i - \zeta_\infty} \quad (6)$$

where $\zeta_\infty = \zeta_p/\sqrt{2}$ is the limiting zeta potential and ζ_p is the zeta potential of the protein in the bulk. The validity of eqs 5 and 6 for interpreting HSA adsorption on mica was confirmed in ref 46.

The experimental data obtained for bovine and human fibrinogens transformed in this way to the N_f vs $t^{1/2}$ relationship are plotted in Figure 3. They are compared with theoretical results calculated by a numerical solution of the diffusion equation with the blocking function derived from the random sequential adsorption model (RSA).^{47–51} As can be observed,

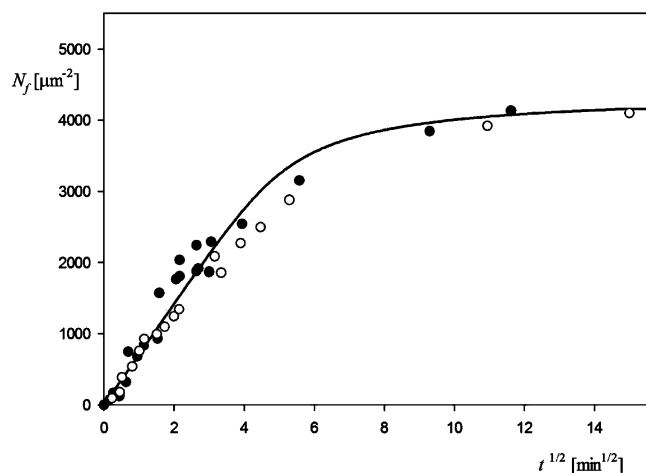


Figure 3. The kinetics of fibrinogen adsorption for the diffusion-controlled adsorption regime. The points represent experimental results determined by streaming potential measurements for mica, $c_b = 10 \text{ mg L}^{-1}$, pH 3.5 and 10^{-2} M , NaCl. The solid line denotes exact theoretical results calculated by solving the diffusion equation for the 3D RSA adsorption model.

the experimental data agree with theoretical results calculated assuming the 3D adsorption, over the entire range of surface concentrations. It is also interesting to mention that for N_f smaller than $3000 \text{ } \mu\text{m}^{-2}$ the surface concentration of fibrinogen N_f is a linear function of the square root of time and can be, therefore, well described by the simple analytical formula derived from eq 4.

$$N_f = 2 \left(\frac{D}{\pi} \right)^{1/2} t^{1/2} n_b \quad (7)$$

where $n_b = c_b (10^{-6} \text{ A}_v/M_w)$ is the number concentration of fibrinogen in the bulk, A_v is Avogadro's constant, and M_w is the molar mass of fibrinogen.

Knowing this, one can express the electrokinetic measurements shown in Figure 3 as the dependence of the zeta potential of mica on the surface concentration of fibrinogen, N_f . Such dependencies derived for different ionic strength are plotted in Figure 4. As can be seen, for the ionic strength of 10^{-2} M , the zeta potential of fibrinogen covered mica becomes positive for $N_f > 1400 \text{ } \mu\text{m}^{-2}$, that is usually interpreted as the overcharging effect. This critical N_f value is similar for lower ionic strength of $3 \times 10^{-4} \text{ M}$. It is interesting to mention that the experimental results shown in Figure 4 are well approximated by the electrokinetic model (depicted by solid lines) developed in ref 41.

However, one should mention that the zeta potential plotted in Figure 4 represents a mean-field quantity having a proper interpretation for surface areas considerably exceeding the fibrinogen molecule surface area. For smaller areas, the heterogeneity of charge distribution in fibrinogen monolayers that depends on molecule orientations should play an essential role. These effects can be evaluated via colloid particle deposition measurements discussed next.

3.3. Latex Particle Deposition on Fibrinogen Monolayers. In order to determine fibrinogen orientation in monolayers, latex deposition experiments were performed according to the above-described procedure. These studies were performed under diffusion-controlled conditions at pH 3.5 and various ionic strength. The number of latex particles

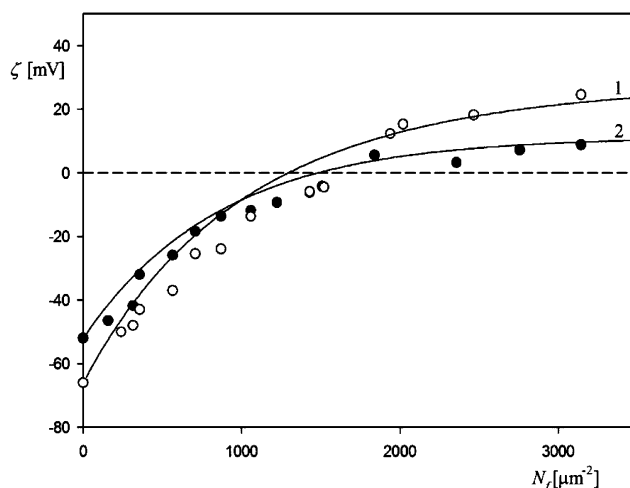


Figure 4. Dependencies of the zeta potential of mica ζ on the surface concentration of human fibrinogen N_f (adsorbed at pH 3.5, 10^{-2} M , NaCl). The points denote experimental results obtained from the streaming potential measurements for different ionic strength: (○) $I = 10^{-2} \text{ M}$, (●) $I = 3 \times 10^{-4} \text{ M}$. The solid lines 1 and 2 represent exact theoretical results calculated from the 3D electrokinetic model developed in refs 49 and 50.

adsorbed as a function of deposition time was determined via the direct counting procedure using optical microscopy and AFM.

An advantage of optical microscopy is that it enables measurements to be carried out under wet conditions, where particle positions over the substrate surface remain undisturbed. This allows one to reliably determine not only the coverage of particles but also their distributions over bare and fibrinogen covered substrates.

The procedure for determining latex coverage was as described above. In the first stage, fibrinogen monolayers of an appropriate coverage (determined by AFM and streaming potential measurements) were produced on mica sheets under diffusion transport conditions. Afterward, the wet sheets were immersed in the latex suspension having the bulk concentration of $1.77 \times 10^{10} \text{ cm}^{-3}$. After completing the deposition run lasting 24 h, the latex surface concentration N_l was determined by direct optical microscopy imaging (wet conditions) and AFM imaging (in air). The statistical uniformity of latex particle distributions on mica covered fibrinogen was confirmed using variance analysis of the number of particles deposited over equal-sized surface areas. One should mention that, in all these experiments, latex deposition was irreversible, which was confirmed in separate desorption runs, where the covered mica sheets were immersed for a prolonged time period (48 h) in pure electrolyte having the same ionic strength and pH. The coverage of latex was monitored by in situ optical microscope observations.

In order to facilitate a proper interpretation of these experiments, a series of calibration runs was performed where the deposition kinetics of positive amidine latex A800 particles of the same size as the L800 negative latex, i.e., 820 nm on bare mica was determined. The results of these experiments are shown in Figure 5 (pH 3.5, 10^{-2} M , NaCl) as the dependence of latex coverage Θ_l on the square root of the deposition time $t^{1/2}$. As can be seen, the experimental data (full points) are well reflected by the theoretical results calculated by numerically solving the governing transport equation using the blocking

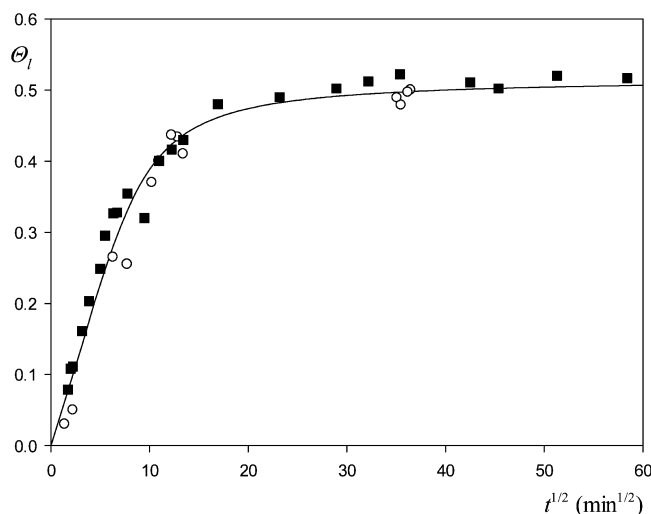


Figure 5. Kinetics of the L800 latex particle deposition on mica covered by (○) bovine fibrinogen monolayer $N_f = 2000 \mu\text{m}^{-2}$, pH 3.5, 10^{-2} M, NaCl, (AFM, SEM measurements). (■) Results obtained for the positive amidine latex A800 (average diameter 800 nm) deposition on bare mica at the same conditions. The solid line denotes the theoretical results calculated from the RSA model for diffusion-controlled transport.

function derived from the random sequential adsorption (RSA) approach.^{44,45} Analogous kinetic runs carried out for the L800 (negative) latex on fibrinogen covered mica for $N_f = 2000 \mu\text{m}^{-2}$, pH 3.5, and 10^{-2} M, NaCl are also shown in Figure 5. As can be noticed, they agree with the previous reference results obtained for the positive latex on bare mica. This indicates that, in the limit of high fibrinogen coverage, the latex particle deposition kinetics is quite analogous as for bare surfaces.

After proving this, a series of experiments was performed where the dependence of the maximum L800 latex coverage Θ_l (attained after 24 h) on the fibrinogen surface concentration N_f was systematically studied. The results obtained in these experiments for bovine (filled points) and human fibrinogen (hollow points) are shown in Figure 6b (pH 3.5 and 10^{-2} M, NaCl). As can be seen, the latex coverage increases abruptly with the fibrinogen surface concentration attaining half of its maximum value for N_f as small as $250 \mu\text{m}^{-2}$. For $N_f > 1000 \mu\text{m}^{-2}$, the latex coverage almost matches its maximum value pertinent to 24 h adsorption. The same trend is observed for the human fibrinogen.

It should be mentioned that the experimental data shown in Figure 6b are anomalous compared to measurements of colloid particle deposition on homogeneous surfaces.^{41,44} This becomes evident if one notes that, for pH 3.5 and $N_f < 1400 \mu\text{m}^{-2}$, where a significant latex deposition is measured, the mean-field zeta potential of the fibrinogen covered mica is negative (see Figure 4), that is, of the same sign as the zeta potential of latex. According to classical views, this should result in a strong electrostatic repulsion between particles and the substrate preventing deposition.

Therefore, it is instructive to analyze this discrepancy by comparing the experimental data with theoretical results stemming from the standard DLVO model. The main assumption of this theoretical approach is that the van der Waals and electric double-layer interactions are additive, which can be expressed for the spherical particle/flat interface by the equation³⁴

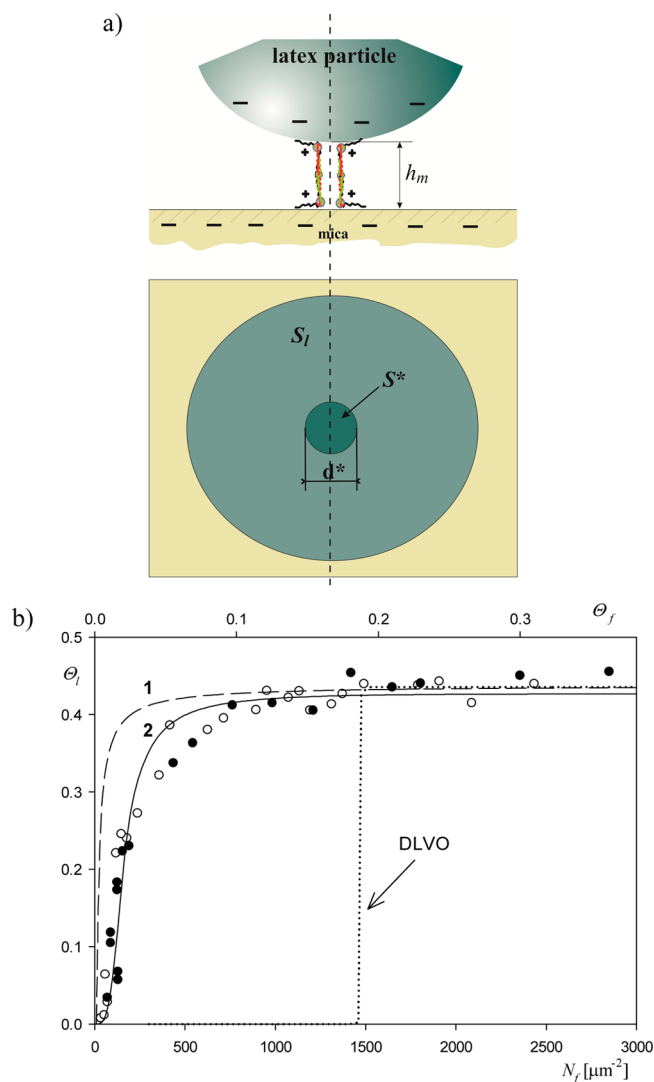


Figure 6. (a) Schematic view of fibrinogen molecules forming an adsorption site. S^* is the interaction area, S_l is the latex particle cross-section area, and h_m is the minimum approach distance of latex to mica. (b) Dependence of the L800 latex particle coverage attained after 24 h (bulk latex concentration $1.77 \times 10^{10} \text{ cm}^{-3}$, pH 3.5, 10^{-2} M NaCl) on the fibrinogen surface concentration $N_f [\mu\text{m}^{-2}]$. The points denote the experimental results obtained by optical microscopy and AFM for bovine (●) and human (○) fibrinogens. The solid lines 1 and 2 represent theoretical results derived from the fluctuation theory, eqs 12 and 14, assuming latex deposition on end-on oriented fibrinogen molecules, forming adsorption sites composed of at least one and at least two molecules, respectively. The dashed line shows the mean-field results calculated from the DLVO theory.

$$\phi(h) = -\frac{A_{123}d_l}{3h} + \phi_0 e^{-\kappa h} \quad (8)$$

where $\phi(h)$ is the interaction energy, A_{123} is the Hamaker constant for the polystyrene/water/mica interactions, h is the gap between the particle, and the interface $\phi_0 = 64\pi\epsilon d_l(kT/e)^2 \tanh(\zeta_e/4kT) \tanh(\zeta_i/4kT)$ is the characteristic energy for the linear superposition approximation (LSA) double-layer model.^{52,53} $\kappa^{-1} = (\epsilon kT/2e^2 I)^{1/2}$ is the electrical double layer thickness.

Assuming a typical value of $A_{123} = 5 \times 10^{-14} kT$, $\zeta = -15$ mV (for fibrinogen surface concentration of $250 \mu\text{m}^{-2}$), $\zeta_i = -100$ mV (see Table 2), and 10^{-2} M NaCl, one obtains from eq 8

that $\phi = 105 kT$ for $h = 7$ nm (fibrinogen diameter in the side-on configuration) and $\phi = 1.5 kT$ for $h = 20$ nm. It should be mentioned the energy calculated as above is mainly governed by the electrostatic interactions.

This estimation shows that, by assuming the mean-field zeta potential, an energy barrier of a considerable height and thickness $\delta_b = 20$ nm should appear for the fibrinogen coverage below $1400 \mu\text{m}^{-2}$. Knowing the energy distribution, one can calculate the adsorption rate constant from the formula^{44,45}

$$k_a = \left[\int_{\delta_b} \frac{e^{\phi(h)/kT}}{D(h)} dh \right]^{-1} \quad (9)$$

where $D(h)$ is the position dependent diffusion coefficient of the latex particles. Knowing k_a , the latex coverage as a function of deposition time and bulk concentration can be theoretically calculated by solving the governing diffusion equation using the finite-difference scheme as previously described.⁴⁴

It is interesting to mention that, for a barrier height exceeding $10 kT$ (which is the case for the mean-field zeta potential below -2 mV), the kinetics of latex particle deposition can be approximated by the expression³⁴

$$\Theta_l = S_l k_a n_b t \cong \frac{1}{2} \frac{D}{d_l} \left(\frac{\phi_b}{\pi kT} \right)^{1/2} e^{-\phi_b/kT} S_l n_b t \quad (10)$$

The results calculated using eqs 8–10, referred to as the DLVO theory predictions, are shown by the dashed line in Figure 6b. As can be seen, a negligible latex particle deposition is predicted for the fibrinogen coverage below $1400 \mu\text{m}^{-2}$. This disagrees with experimental results where a significant latex particle deposition was observed for N_f as low as $100 \mu\text{m}^{-2}$.

It is interesting to mention that such deviations from the DLVO theory were before observed for heterogeneous surfaces produced by controlled cationic polyelectrolyte adsorption^{30–33} and for bovine fibrinogen adsorption.^{34,39} They were theoretically analyzed in ref 54 using the grid surface integration (GSI) technique. Both the surface roughness effect and charge heterogeneity were quantitatively evaluated. The surface heterogeneities were introduced in the form of nanopillars having opposite sign of zeta potential compared to the surface and colloid particles. A significant decrease in the energy barrier height with the size of the nanopillars was predicted for their coverage of 0.25. This seems in qualitative accordance with our experimental observations shown in Figure 6. However, the effect of the nanopillar coverage has not been studied. This prohibits a quantitative comparison with our experimental data.

In this work, we quantitatively interpret this discrepancy in terms of the random site adsorption model developed by Jin et al.⁵⁵ and extended in ref 56 by considering finite size of sites. The core assumption of this model is that the sites are randomly distributed over a homogeneous surface and one site is capable of immobilizing only one particle. By introducing the surface concentration of sites N_s , one can define the following parameter, reflecting the number of sites within the interaction area S^* , referred also to as the zone of influence³² shown in Figure 6a

$$\alpha = S^* N_s \quad (11)$$

Jin et al.⁵⁵ assumed that S^* is equal to the cross-section of the particle.

Knowing α , one can calculate the maximum coverage of particles on a surface covered by sites from the analytical dependence³⁴

$$\Theta_l = \Theta_{\text{mx}} \left(1 - \frac{1 + 0.314\alpha^2 + 0.45\alpha^3}{1 + \frac{1}{\Theta_{\text{mx}}}\alpha + 0.66\alpha^3 + \alpha^{7/2}} \right) \quad (12)$$

where Θ_{mx} is the maximum coverage of particles in the limit of high coverage of sites. In our case of latex particle deposition, Θ_{mx} can be derived from the calibration experiments performed for the positive latex and is shown in Figure 5.

As can be deduced from eqs 11 and 12, in order to theoretically calculate the latex coverage, one should express the surface concentration of sites N_s in terms of the fibrinogen surface concentration N_f . For a site formed by a single molecule of the dimension negligible compared with the particle size, $S^* = S_l$, $N_s = N_f$ and α becomes

$$\alpha = S_l N_f = \lambda^2 \Theta_f \quad (13)$$

where $\lambda^2 = S_l/S_g$, S_g is the fibrinogen characteristic cross-section, and $\Theta_f = S_g N_f$ is the fibrinogen coverage.

If particle immobilization occurs on sites formed by n_s or more closely spaced molecules, the following equation can be derived assuming that the site distribution is governed by the Poisson statistics³⁰

$$\alpha(n_s) = \lambda^2 \left[1 - e^{-\langle N \rangle} \sum_{n=0}^{n_s-1} \frac{\langle N \rangle^n}{n!} \right] \quad (14)$$

where $\langle N \rangle = S^* N_f$ is the average number of single fibrinogen molecules within the interaction area.

In the case of $n_s = 2$ (the site formed by at least two or more fibrinogen molecules as shown in Figure 6a), one can derive from eq 14 the explicit expression

$$\alpha(2) = \lambda^2 [1 - e^{-\langle N \rangle} (1 + \langle N \rangle)] \quad (15)$$

The interaction area S^* can be calculated from simple geometry and is given by the expression

$$S^* = \frac{\pi d_l^2}{4} (2Y - Y^2) \quad (16)$$

where $Y = 2(L_f - h_m)/d_l$, L_f is the effective length of the fibrinogen molecule (see Table 1), and h_m is the minimum approach distance of the latex particle to the substrate surfaces.

Using eq 8 and neglecting the van der Waals interactions, h_m can be expressed as

$$h_m = \kappa^{-1} \ln \left(\frac{\phi_0}{\phi_{\text{ch}}} \right) \quad (17)$$

where ϕ_{ch} is the characteristic interaction energy.

Using the experimental parameters pertinent to the latex/mica system, one can calculate from eq 17 that h_m varies between 19 and 79 nm for ionic strength of 10^{-2} and 6×10^{-4} M, respectively (assuming $\phi_{\text{ch}} = 6 kT$). Therefore, latex deposition for this ionic strength range is only feasible on fibrinogen molecules adsorbed in the end-on orientations, whose extended length with side chains equals 85 nm (see Table 1).

Considering eq 16, one can express the λ^2 parameter as

$$\lambda^2 = \frac{1}{2Y - Y^2} \quad (18)$$

Using eqs 16 and 18 in conjuncture with eq 12, one can explicitly calculate the coverage of latex on sites formed by various number fibrinogen configurations. The surface concentration of end-on adsorbed fibrinogen molecules N_L can be derived from the recent theoretical modeling of fibrinogen adsorption at lower pH values.²⁹ Analytical expressions were derived in this work for interpolation of the numerical data. For $N_f < 1000 \mu\text{m}^{-2}$, one derives the formula

$$N_L = c_1 N_f + c_2 N_f^2 - c_3 N_f^3 \quad (19)$$

where $c_1 = 0.036$, $c_2 = 9.00 \times 10^{-4}$, and $c_3 = 3.3 \times 10^{-7}$.

Analogous interpolations were derived for $10^3 \mu\text{m}^{-2} < N_f < 7 \times 10^3 \mu\text{m}^{-2}$:

$$N_L = c'_0 + c'_1(N_f - 1000) \quad (20)$$

where $c'_0 = 606$ and $c'_1 = 0.987$.

The prevailing end-on conformation of fibrinogen molecules was experimentally confirmed in ref 28 where the maximum coverage of fibrinogen on latex particles was determined for various ionic strength and pH 3.5. However, these measurements do not allow one to prove the end-on conformation of fibrinogen molecules for the low coverage range.

Using eqs 19 and 20, one can calculate the $\alpha(n_s)$ parameter and subsequently the latex coverage as a function of N_f using eq 12. The theoretical calculations in this way for $n_s = 1$ (latex deposition on single fibrinogen molecules) and 2 (adsorption on at least two fibrinogen molecules) are plotted in Figure 6b (lines 1 and 2, respectively). As can be seen, the experimental data disagree with theoretical results derived for $n_s = 1$, since a much steeper increase of Θ_1 with N_f is theoretically predicted. This indicates that immobilization of latex particles on sites consisting of a single fibrinogen molecule was not possible due to too low attractive interaction energy.

The energy can be calculated by considering the discrete electrostatic interactions among ion pairs on the side arms of the fibrinogen molecule and latex particles. As shown in ref 57, the interaction energy per one such ion pair is $-1.4 kT$. Assuming that the number of ion pairs equals one-half of N_c , that is, 10 in the case of 10^{-2} M (see Table 2), the net interaction energy per one fibrinogen molecule ϕ_0 equals $-14 kT$. Considering that the diffusion coefficient of latex D_L is $6 \times 10^{-9} \text{ cm}^2 \text{ s}^{-1}$, one can calculate that the characteristic relaxation time of particle desorption is 8.5 s.⁴⁵ Since this is considerably smaller than the time of experiments (86 400 s), the possibility of latex immobilization by one fibrinogen molecule is unequivocally excluded. On the other hand, for immobilization on the site formed by two fibrinogen molecules, the relaxation time increases to 10^7 seconds, that is practically infinite from an experimental point of view.

An analogous behavior was previously observed in the case of poly(allylamine) hydrochloride and poly(ethylene imine) polyelectrolytes,^{30,31} where latex particle deposition occurred at adsorption sites composed of two or more closely spaced polyelectrolyte chains.

An irreversible immobilization of latex particles by at least two fibrinogen molecules theoretically predicted agrees with experimental data shown in Figure 6b (curve 2), obtained for $n_s = 2$. Hence, the results shown in Figure 6b suggest that eqs 19 and 20 adequately describe the surface concentration of end-on oriented fibrinogen molecules, especially at the lower range of

$N_f < 500 \mu\text{m}^{-2}$. This also validates the end-on mechanisms of fibrinogen adsorption at lower range of surface concentrations suggested in the above work of Cieřla et al.²⁹ Additionally, the large slope of the Θ_1 vs N_f dependence shown in Figure 6b (where a half of the maximum latex coverage is attained for N_f as low as $200 \mu\text{m}^{-2}$) suggests that the bulk concentration of fibrinogen can be sensitively determined via the latex deposition procedure. Given the high accuracy of determining the latex coverage at the level of 0.001 (0.1%), this seems an attractive alternative compared to the bulk chemical methods requiring protein quantities exceeding 0.1 mg. However, as can be seen in Figure 6a, the sensitivity of the latex deposition method becomes limited for N_f higher than $500 \mu\text{m}^{-2}$. This is not a serious limitation of the applicability of the method because one can always dilute in a controlled way the fibrinogen sample in order to obtain the concentration within the high sensitivity region.

Additional series of experiments were performed in order to elucidate the role of ionic strength at a fixed pH 3.5. The results of these experiments are shown in Figure 7. As can be seen, all

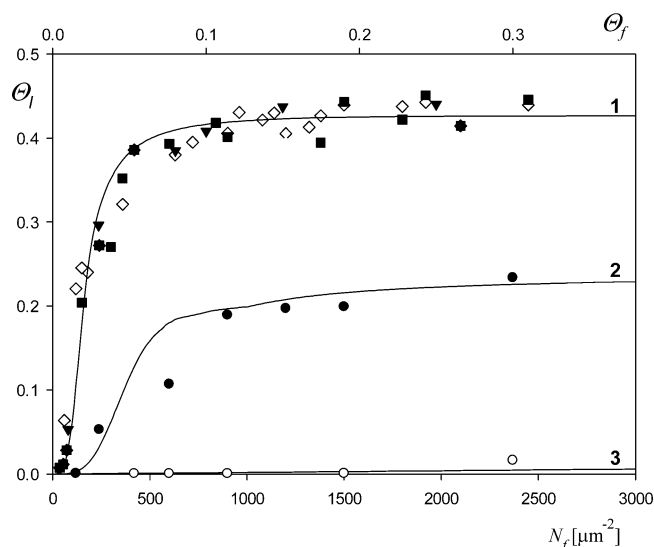


Figure 7. Dependence of the coverage of latex particles, Θ_1 on the bovine fibrinogen surface concentration $N_f [\mu\text{m}^{-2}]$, pH 3.5. The points denote the averaged experimental results obtained by optical microscopy and AFM for pH various ionic strength: (\blacktriangledown) 0.15 M, (\diamond) 10^{-2} M, (\blacksquare) 10^{-3} M, (\bullet) 6×10^{-4} M, and (\circ) 3×10^{-4} M. Solid lines 1–3 show theoretical prediction derived from the fluctuation theory, eqs 12 and 14, assuming deposition of latex on sites formed by at least two fibrinogen molecules.

results obtained for ionic strength within the range $0.15\text{--}10^{-3}$ M are identical within experimental error bounds, and can be adequately reflected by the above theoretical model (eqs 12, 14, and 18) assuming $n_f = 2$. However, for lower ionic strength of 6×10^{-4} M, the latex deposition efficiency significantly decreases and vanishes for 3×10^{-4} M. This behavior unequivocally confirms a dominant role of the electrostatic interactions in latex particle deposition on fibrinogen monolayers. Similarly as in the previous case (see Figure 6b) the mean-field theory is inadequate to explain this behavior. This is evident if one notices that for $N_f > 1400 \mu\text{m}^{-2}$ and all ionic strength the average zeta potential of mica covered by fibrinogen becomes positive but a negligible latex deposition is observed.

Analogous results were reported by Duffadar et al.³² In this work, initial deposition rates of silica particles on the cationic polyelectrolyte pDMAEMA monolayers preadsorbed to a controlled degree on microscope slides at pH 6.1 were studied. A significant decrease in the initial deposition rate was observed for decreasing ionic strength. However, for the low ionic strength (where $\kappa^{-1} = 10$ nm) and high polyelectrolyte coverage, the results were in agreement with the DLVO theory. Similar data were also discussed in ref 33 where silica particle deposition on fibrinogen covered silica slides was studied by video microscopy at pH 7.4. In this case, the threshold value for silica particle deposition was roughly $1000 \mu\text{m}^{-2}$ for ionic strength of 2.6×10^{-2} M and $1500 \mu\text{m}^{-2}$ for ionic strength of 0.005 M. Again, in the limit of high fibrinogen coverage, the results were in accordance with the DLVO theory. These differences stem probably from the fact that our deposition experiments lasted 24 h, whereas the kinetic experiments of Kalasin and Santore³³ were performed under convection conditions (in the parallel-plate channel) and lasted typically 5 min. These conditions were, therefore, less favorable for an effective attachment of silica particles under strong shearing forces prevailing at the channel's walls. Another plausible explanation is that, as assumed in these works, polyelectrolyte and fibrinogen monolayers were formed of mostly side-on oriented molecules.

The influence of the ionic strength on latex deposition efficiency is quantitatively presented in Figure 8, as the

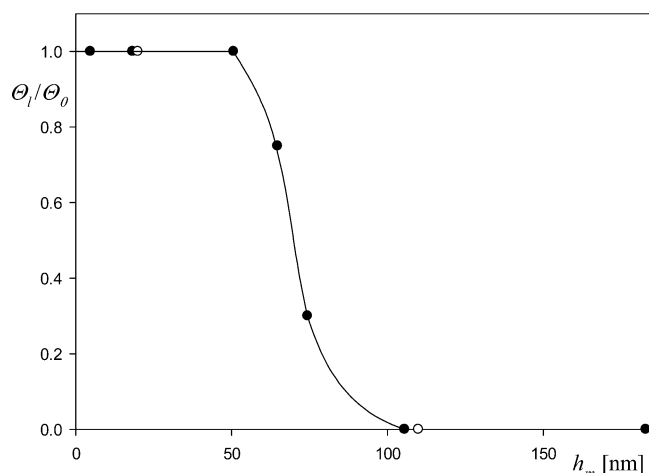


Figure 8. Dependence of the normalized coverage of the latex particles, Θ_i/Θ_0 , on the effective interaction range h_m . The points denote the experimental results obtained by optical microscopy and AFM (averaged) for bovine (●) and human (○) fibrinogens. The solid line is the nonlinear fit of experimental data.

normalized latex coverage Θ_i/Θ_0 (where Θ_0 is the latex coverage after 24 h obtained for $N_i = 2000 \mu\text{m}^{-2}$) vs the minimum approach distance h_m calculated from eq 17. As can be seen, Θ_i/Θ_0 decreases abruptly for $h_m > 50$ nm and for $h_m = 75$ nm equals to half of its initial value. This threshold distance considerably exceeds not only the length of the core part of the fibrinogen molecule equal to 49.7 nm (see Table 1) but also its extended length with one arm fully stretched at 75 nm.

Therefore, the results shown in Figure 8 not only confirm the end-on adsorption mechanism of fibrinogen on mica but also the fact that the positive charge is concentrated in the end parts of the A α chains (side arms). This was previously predicted in

refs 39 and 58 where the dynamic viscosity and DLS measurements combined with theoretical calculations were applied for deriving fibrinogen conformations. In view of this experimental evidence, one can conclude that the colloid deposition method is a convenient and efficient tool for studying orientations and charge distribution of adsorbed fibrinogen molecules.

4. CONCLUDING REMARKS

It was confirmed by direct AFM measurements that fibrinogen molecules irreversibly adsorb on mica at pH 3.5 with the rate controlled by the bulk transport.

The electrokinetic properties of the fibrinogen monolayers for various ionic strength were characterized in terms of the streaming potential measurements, enabling one to determine the mean-field zeta potential.

The orientation of adsorbed fibrinogen molecules was quantitatively determined using the colloid deposition method. An anomalous deposition of negative latex particles on substrates exhibiting a negative mean-field zeta potential was confirmed that is contradicting the DLVO theory.

Results of these experiments were properly interpreted in terms of the fluctuation theory assuming that adsorption sites consisted of at least two fibrinogen molecules in the end-on orientation.

The results obtained in this work confirmed not only the validity of the end-on adsorption mechanism of fibrinogen on mica theoretically predicted in ref 29 but also the fact that the positive charge is concentrated in the end parts of the A α chains. This exerts a decisive influence on deposition phenomena promoting immobilization of negatively charged particles on surfaces covered by fibrinogen monolayers.

Therefore, the results obtained in our model system can be of interest for predicting mechanism of biofilm formation and bioparticle immobilization, for example, bacteria, induced by fibrinogen adsorption.

It was also concluded that the colloid deposition method can be used for a quantitative determination of the fibrinogen bulk concentration, for a range inaccessible for other methods.

AUTHOR INFORMATION

Corresponding Author

*E-mail: nccadamcz@cyf-kr.edu.pl. Phone: (48)(12) 6395104. Fax: (48)(12) 4251923.

Notes

The authors declare no competing financial interest.

ACKNOWLEDGMENTS

This work was supported by the NCN Grant UMO-2012/07/B/ST4/00559

REFERENCES

- (1) Nakanishi, K.; Sakiyama, T.; Imamura, K. On the adsorption of proteins on solid surfaces, a common but very complicated phenomenon. *J. Biosci. Bioeng.* **2001**, *91*, 233–244.
- (2) Gorbet, M. B.; Sefton, M. V. Biomaterial-associated thrombosis: roles of coagulation factors, complement, platelets and leukocytes. *Biomaterials* **2004**, *25*, 5681–5703.
- (3) Grunkemeier, J. M.; Tsai, W. B.; McFarland, C. D.; Horbett, T. A. The effect of adsorbed fibrinogen, fibronectin, von Willebrand factor and vitronectin on the procoagulant state of adherent platelets. *Biomaterials* **2000**, *21*, 2243–2252.

- (4) Hantagan, R. R.; Simpson-Haidaris, P. J.; Francis, C. W.; Marder, V. J. Fibrinogen Structure and Physiology. In *Hemostasis and Thrombosis: Basic Principles and Clinical Practice*; Colman, R. W., Hirsh, J., Marder, V. J., Clowes, A. W., George, J., Eds.; Lippincott Williams & Wilkins: Philadelphia, 2000; pp 203–232.
- (5) Lewis, K. B.; Ratner, B. D. Imaging fibrinogen adsorbed on noble metal surfaces with scanning tunneling microscopy: correlation of images with electron spectroscopy for chemical analysis, secondary ion mass spectrometry, and radiolabeling studies. *Colloids Surf., B* **1996**, *7*, 259–269.
- (6) Herrick, S.; Blanc-Brude, O.; Gray, A.; Laurent, G. Fibrinogen. *IJBCB* **1999**, *31*, 741–746.
- (7) Mosesson, M. W. Fibrinogen and fibrin structure and functions. *J. Thromb. Haemostasis* **2005**, *3*, 1894–1904.
- (8) Watt, K. W. K.; Takagi, T.; Doolittle, R. F. Amino acid sequence of the β chain of human fibrinogen: homology with the γ chain. *Proc. Natl. Acad. Sci. U.S.A.* **1978**, *75*, 1731–1735.
- (9) Jung, S. Y.; Lim, S. M.; Albertorio, F. The Vroman effect: A molecular level description of fibrinogen displacement. *J. Am. Chem. Soc.* **2003**, *125*, 12782–12786.
- (10) Hall, C. E.; Slayter, H. S. The fibrinogen molecule: its size, shape and mode of polymerization. *J. Biophys. Biochem. Cytol.* **1959**, *5*, 11–16.
- (11) Fowler, W. E.; Erickson, H. P. Trinodular structure of fibrinogen: Confirmation by both shadowing and negative stain electron microscopy. *J. Mol. Biol.* **1979**, *134*, 241–249.
- (12) Weisel, J. W.; Stauffacher, C. V.; Bullitt, E.; Cohen, C. A model for fibrinogen: domains and sequence. *Science* **1985**, *230*, 1388–1391.
- (13) Veklich, Y. J.; Gorkun, O. V.; Medved, L. V.; Nieuwenhuizen, W.; Weisel, J. W. Carboxyl-terminal portions of the alpha chains of fibrinogen and fibrin. Localization by electron microscopy and the effects of isolated alpha C fragments on polymerization. *J. Biol. Chem.* **1993**, *268*, 13577–13585.
- (14) Ortega-Vinuesa, J. L.; Tengvall, P. I.; Lundström, I. Molecular packing of HSA, IgG, and fibrinogen adsorbed on silicon by AFM imaging. *Thin Solid Films* **1998**, *324*, 257–273.
- (15) Ortega-Vinuesa, J. L.; Tengvall, P.; Lundström, I. Aggregation of HSA, IgG, and Fibrinogen on Methylated Silicon Surfaces. *J. Colloid Interface Sci.* **1998**, *207*, 228–239.
- (16) Sit, P. S.; Marchant, R. E. Surface-dependent conformations of human fibrinogen observed by atomic force microscopy under aqueous conditions. *J. Thromb. Haemostasis* **1999**, *82*, 1053–1060.
- (17) Marchin, K. L.; Berrie, C. L. Conformational changes in the plasma protein fibrinogen upon adsorption to graphite and mica investigated by atomic force microscopy. *Langmuir* **2003**, *19*, 9883–9888.
- (18) Ishizaki, T.; Saito, N.; Suto, X.; Takai, O. Probing into adsorption behavior of human plasma fibrinogen on self-assembled monolayers with different chemical properties by scanning probe microscopy. *Surf. Sci.* **2007**, *601*, 3861–3865.
- (19) Tunc, S.; Maitz, M. F.; Steiner, G.; Vazquez, L.; Pham, M. T.; Salzer, R. In situ conformational analysis of fibrinogen adsorbed on Si surfaces. *Colloids Surf., B* **2005**, *42*, 219–225.
- (20) Toscano, A.; Santore, M. M. Fibrinogen adsorption on three silica-based surfaces: conformation and kinetics. *Langmuir* **2006**, *22*, 2588–2597.
- (21) Young, B. R.; Pitt, W. G.; Cooper, S. L. Protein Adsorption on Polymeric Biomaterials. I. Adsorption Isotherms. *J. Colloid Interface Sci.* **1988**, *124*, 28–43.
- (22) Bai, Z.; Filiaggi, M. J.; Dahn, J. R. Fibrinogen adsorption onto 316L stainless steel, Nitinol and titanium. *Surf. Sci.* **2009**, *603*, 839–846.
- (23) Berglin, M.; Pinori, E.; Sellborn, A.; Andersson, M.; Hulander, M.; Elwing, H. Fibrinogen adsorption and conformational change on model polymers: Novel aspects of mutual molecular rearrangement. *Langmuir* **2009**, *25*, 5602–5608.
- (24) Malmsten, M. Ellipsometry studies of protein layers adsorbed at hydrophobic surfaces. *J. Colloid Interface Sci.* **1994**, *166*, 333–342.
- (25) Wertz, Ch.F.; Santore, M. M. Effect of surface hydrophobicity on adsorption and relaxation kinetics of albumin and fibrinogen: single-species and competitive behaviour. *Langmuir* **2001**, *17*, 3006–3016.
- (26) Santore, M. M.; Wertz, Ch.F. Protein spreading kinetics at liquid-solid interfaces via an adsorption probe method. *Langmuir* **2005**, *21*, 10172–10178.
- (27) Dyr, J. E.; Suttner, J. Molecular arrangement of adsorbed fibrinogen molecules characterized by specific monoclonal antibodies and a surface plasmon resonance sensor. *Sen. Actuators, B* **1998**, *51*, 268–272.
- (28) Bratek-Skicki, A.; Żeliszewska, P.; Adamczyk, Z.; Cieśla, M. Human fibrinogen monolayers on latex particles: role of ionic strength. *Langmuir* **2013**, *29*, 3700–3710.
- (29) Cieśla, M.; Adamczyk, Z.; Barbasz, J.; Wasilewska, M. Mechanisms of fibrinogen adsorption at solid substrates at lower pH. *Langmuir* **2013**, *29*, 7005–7016.
- (30) Adamczyk, Z.; Zembala, M.; Michna, A. Polyelectrolyte adsorption layers studied by streaming potential and particle deposition. *J. Colloid Interface Sci.* **2006**, *303*, 353–364.
- (31) Adamczyk, Z.; Michna, A.; Szaraniec, M.; Bratek, A.; Barbasz, J. Characterization of poly(ethylene imine) layers on mica by the streaming potential and particle deposition methods. *J. Colloid Interface Sci.* **2007**, *313*, 86–96.
- (32) Duffadar, R.; Kalasin, S.; Davis, J. M.; Santore, M. M. The impact of nanoscale chemical features on micron-scale adhesion: Crossover from heterogeneity-dominated to mean-field behavior. *J. Colloid Interface Sci.* **2009**, *337*, 396–407.
- (33) Kalasin, S.; Santore, M. M. Non-specific adhesion on biomaterial surfaces driven by small amounts of protein adsorption. *Colloids Surf., B* **2009**, *73*, 229–236.
- (34) Adamczyk, Z.; Nattich, M.; Wasilewska, M.; Sadowska, M. Deposition of colloid particles on protein layers: Fibrinogen on mica. *J. Colloid Interface Sci.* **2011**, *356*, 454–464.
- (35) Smith, P. K.; Krohn, R. I.; Hermanson, G. T.; Mallia, A. K.; Gartner, F. H.; Provenzano, M. D.; Fujimoto, E. K.; Goeke, N. M.; Olson, B. J.; Klenk, D. C. Measurement of protein using bicinchoninic acid. *Anal. Biochem.* **1985**, *150*, 76–85.
- (36) Goodwin, J. W.; Hearn, J.; Ho, C. C.; Ottewill, R. H. Studies on the preparation and characterization of monodisperse polystyrene latices. III. Preparation without added surface active agents. *Colloid Polym. Sci.* **1974**, *252*, 464–471.
- (37) Zembala, M.; Adamczyk, Z. Measurements of streaming potential for mica covered by colloid particles. *Langmuir* **2000**, *16*, 1593–1601.
- (38) Adamczyk, Z.; Zaucha, M.; Zembala, M. Zeta potential of mica covered by colloid particles: A streaming potential study. *Langmuir* **2010**, *26*, 9368–9377.
- (39) Wasilewska, M.; Adamczyk, Z. Fibrinogen adsorption on mica studied by AFM and in situ streaming potential measurements. *Langmuir* **2011**, *27*, 686–696.
- (40) Zembala, M.; Adamczyk, Z.; Warszński, P. Influence of adsorbed particles on streaming potential of mica. *Colloids Surf., A* **2001**, *195*, 3–15.
- (41) Adamczyk, Z.; Sadlej, K.; Wajnryb, E.; Nattich, M.; Ekiel-Jezewska, M. L.; Bławdziewicz, J. Streaming potential studies of colloid, polyelectrolyte and protein deposition. *Adv. Colloid Interface Sci.* **2010**, *153*, 1–29.
- (42) Wasilewska, M.; Adamczyk, Z.; Jachimska, B. Structure of fibrinogen in electrolyte solutions derived from dynamic light scattering (DLS) and viscosity measurements. *Langmuir* **2009**, *25*, 3698–3704.
- (43) Tsapikouni, T. S.; Missirlis, Y. F. pH and ionic strength effect on single fibrinogen molecule adsorption on mica studied with AFM. *Colloids Surf., B* **2007**, *57*, 89–96.
- (44) Adamczyk, Z. Kinetics of diffusion-controlled adsorption of colloid particles and proteins. *J. Colloid Interface Sci.* **2000**, *229*, 477–489.

- (45) Adamczyk, Z. *Particles at interfaces: Interactions, deposition, structure*; Elsevier/Academic Press: Amsterdam, 2006; pp 214–219.
- (46) Dąbkowska, M.; Adamczyk, Z.; Kujda, M. Mechanism of HSA adsorption on mica determined by streaming potential, AFM and XPS measurements. *Colloids Surf., B* **2013**, *101*, 442–449.
- (47) Hinrichsen, E. L.; Feder, J.; Jøssang, T. Geometry of random sequential adsorption. *J. Stat. Phys.* **1986**, *44*, 793–827.
- (48) Schaaf, P.; Talbot, J. Surface exclusion effects in adsorption processes. *J. Chem. Phys.* **1989**, *91*, 4401–4409.
- (49) Evans, J. W. Random and cooperative sequential adsorption. *Rev. Mod. Phys.* **1993**, *65*, 1281–1329.
- (50) Talbot, J.; Tarjus, G.; van Tassel, P. R.; Viot, P. From car parking to protein adsorption: an overview of sequential adsorption process. *Colloids Surf., A* **2000**, *165*, 287–324.
- (51) Adamczyk, Z.; Weroński, P. Random sequential adsorption of spheroidal particles: kinetics and jamming limit. *J. Chem. Phys.* **1996**, *105*, 5562–5573.
- (52) Adamczyk, Z.; Warszyński, P. Role of electrostatic interactions in particle adsorption. *Adv. Colloid Interface Sci.* **1996**, *63*, 41–149.
- (53) Adamczyk, Z. Particle adsorption and deposition: role of electrostatic interactions. *Adv. Colloid Interface Sci.* **2003**, *100*, 267–347.
- (54) Bendersky, M.; Davis, J. M. DLVO interaction of colloidal particles with topographically and chemically heterogeneous surfaces. *J. Colloid Interface Sci.* **2011**, *353*, 87–97.
- (55) Jin, X.; Wang, N. H. L.; Tarjus, G.; Talbot, J. Irreversible adsorption on nonuniform surfaces: the random site model. *J. Phys. Chem.* **1993**, *97*, 4256–4258.
- (56) Adamczyk, Z.; Weroński, P.; Musiał, E. Irreversible adsorption of hard spheres at random site (heterogeneous) surfaces. *J. Chem. Phys.* **2002**, *116*, 4665–4672.
- (57) Adamczyk, Z.; Barbasz, J.; Cieśla, M. Mechanisms of fibrinogen adsorption at solid substrates. *Langmuir* **2011**, *27*, 6868–6878.
- (58) Adamczyk, Z.; Cichocki, B.; Ekiel-Jezewska, M. L.; Słowicka, A.; Wajnryb, E.; Wasilewska, M. Fibrinogen conformations and charge in electrolyte solutions derived from DLS and dynamic viscosity measurements. *J. Colloid Interface Sci.* **2012**, *385*, 244–257.
- (59) RCSB Protein Data Bank, <http://www.pdb.org>.